

# DeltaGAN: Towards Diverse Few-shot Image Generation with Sample-Specific Delta

Yan Hong, Li Niu, Jianfu Zhang, and Liqing Zhang

**Abstract**—Learning to generate new images for a novel category based on only a few images, named as few-shot image generation, has attracted increasing research interest. Several state-of-the-art works have yielded impressive results, but the diversity is still limited. In this work, we propose a novel Delta Generative Adversarial Network (DeltaGAN), which consists of a reconstruction subnetwork and a generation subnetwork. The reconstruction subnetwork captures intra-category transformation, *i.e.*, “delta”, between same-category pairs. The generation subnetwork generates sample-specific “delta” for an input image, which is combined with this input image to generate a new image within the same category. Besides, an adversarial delta matching loss is designed to link the above two subnetworks together. Extensive experiments on six benchmark datasets demonstrate the effectiveness of our proposed method.

**Index Terms**—Few-Shot Image Generation, Transfer Learning, Generative Adversarial Network.

## I. INTRODUCTION

With the great success of deep learning, existing deep image generation models [1], [2], [3], [4], [5], [6], [7], [8], [9], [10], [11] based on Variational Auto-Encoder (VAE) [12] or Generative Adversarial Network (GAN) [13] have made a significant leap forward for generating diverse and realistic images for a given category. However, these methods require amounts of training images to generate new images for a given category, which may fail in adapting to long-tail or newly emerging categories with only a few images. Therefore, given a few images from a category, it is necessary to consider how to generate new realistic and diverse images for this category. This scenario is referred to as few-shot image generation [14], [15], [16], which can benefit a lot of downstream tasks like low-data classification and few-shot classification.

Existing few-shot image generation methods resort to seen categories with sufficient training images to train a model, which can be used to generate new images for an unseen category with only a few images. In the training stage, one or more images from one seen category are fed into the model in each training episode, and the training process is supervised by designed loss functions. In the testing stage, given one or more images from each unseen category, the trained model can generate new images for this category in each testing episode. During both training and testing, the images fed into the model as sources to generate new images are dubbed as conditional

images. For brevity, we refer to the images from seen (*resp.*, unseen) categories as seen (*resp.*, unseen) images.

We roughly classify the existing few-shot image generation methods into three categories: optimization-based methods, fusion-based methods, and transformation-based methods. For optimization-based methods, FIGR [14] and DAWSON [17] adopted meta-learning algorithms to generate new images by fine-tuning the trained model with each unseen category, but they can hardly produce sharp and realistic images. For fusion-based methods, GMN [18], MatchingGAN [15], and F2GAN [16] combined matching procedure with generative models to fuse multiple conditional images. However, they can only produce images similar to conditional images, and cannot be applied to one-shot image generation. For transformation-based methods, DAGAN [19] injected random vectors into the generator to produce new images based on one conditional image. However, the network may ignore the injected random vectors and fail to produce diverse images [20].

Following the research line of transformation-based methods, we propose a novel Delta Generative Adversarial Network (DeltaGAN), which can generate new images based on one conditional image by sampling random vectors. Our DeltaGAN is inspired by few-shot feature generation method Delta-encoder [21], in which intra-category transformation (*i.e.*, the difference between two images within the same category) is called “delta”. The main idea of Delta-encoder is shown in Figure 1(a). In the training stage, Delta-encoder learns to extract delta  $\Delta^r$  from same-category pair  $\{X^S, Y^S\}$  of seen categories, in which  $\Delta^r$  is the additional information required to reconstruct  $Y^S$  from  $X^S$ . We refer to  $X^S$  as conditional (source) sample and  $Y^S$  as target sample. In the testing stage, these extracted deltas are applied to a conditional sample  $X^U$  from an unseen category to generate new samples  $\hat{Y}^U$  for this unseen category. However, Delta-encoder is a few-shot feature generation method, which cannot be directly applied to image generation. Besides, Delta-encoder relies on the deltas extracted from same-category training pairs, which does not support stochastic sampling (*i.e.*, sampling random vectors) to generate new samples in the testing stage.

In this paper, we aim to extend Delta-encoder to few-shot image generation which supports stochastic sampling in the testing stage. In this way, we can sample random vectors to generate more diverse images without reaching training data. One simple modification of Delta-encoder to support stochastic sampling is enforcing deltas to follow a prior distribution (*e.g.*, unit Gaussian distribution) with KL divergence loss, so that we can sample random vectors from this prior distribution to generate new images in the testing stage. However, the delta

Yan Hong, Li Niu, Jianfu Zhang, and Liqing Zhang are with the MOE Key Lab of Artificial Intelligence, Department of Computer Science and Engineering, Shanghai Jiao Tong University, Shanghai, China (email: yanhong.sjtu@gmail.com, ustcnewly@sjtu.edu.cn, c.sis@sjtu.edu.cn, zhang-lq@cs.sjtu.edu.cn).

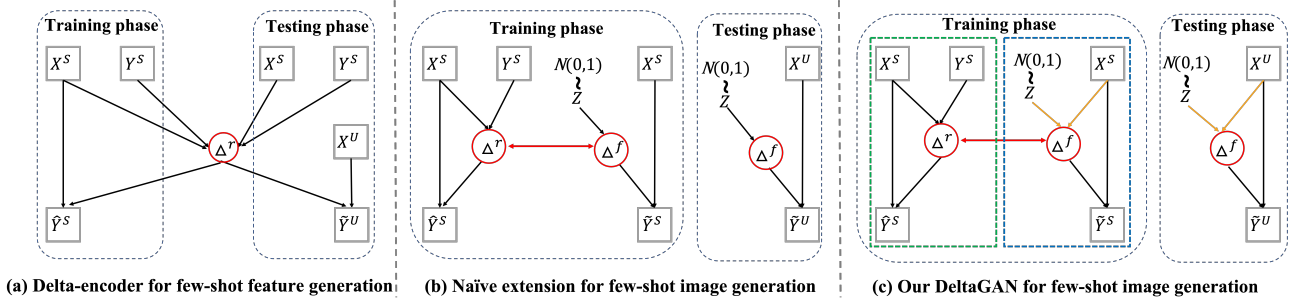


Figure 1: The illustration of evolving from Delta-encoder to our DeltaGAN.  $\{X^S, Y^S\}$  is a same-category seen image pair.  $X^U$  is a conditional image from an unseen category.  $\hat{Y}^S, \hat{Y}^S, \hat{Y}^U$  are generated images.  $z$  is a random vector.  $\Delta^r$  (*resp.*,  $\Delta^f$ ) means real (*resp.*, fake) delta. Red arrows indicate using adversarial delta matching loss to bridge the gap between real and fake delta. In (c), the green (*resp.*, blue) box encloses the reconstruction (*resp.*, generation) subnetwork, and orange arrows indicate the process of generating sample-specific delta.

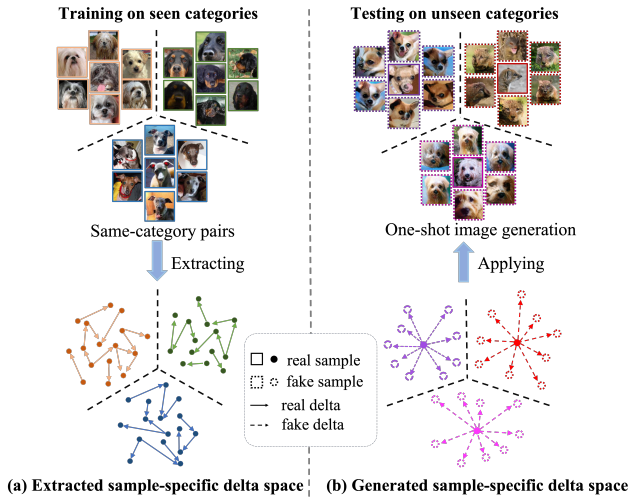


Figure 2: Illustration of our DeltaGAN. In the training stage, we extract real deltas from same-category seen image pairs. In the testing stage, given a conditional unseen image, we generate fake sample-specific deltas for this image to produce diverse and realistic unseen images.

between two images is very informative and imposing a strong prior on the delta may limit its information capacity [22], which leads to the failure of capturing informative deltas (see Section IV-H). Therefore, we turn to learn a mapping from random vector to delta space as shown in Figure 1(b). One concern is that the plausibility of delta may depend on the conditional image [23], that is, a plausible delta for one conditional image may be unsuitable for another conditional image (see Section IV-H).

Due to the above concerns, as shown in Figure 1(c), we take in a random vector and a conditional image to generate sample-specific delta, which represents the transformation from this conditional image to another possible image from the same category. We conjecture that the ability of generating sample-specific delta can be transferred from seen categories to unseen categories. To this end, we develop our DeltaGAN

according to Figure 1(c) and the intuition is also illustrated in Figure 2. In the training phase, we use a reconstruction subnetwork to reconstruct  $Y^S$  from  $X^S$  with the delta  $\Delta^r$  (real delta) extracted from  $\{X^S, Y^S\}$ . We also use a generation subnetwork to generate sample-specific deltas  $\Delta^f$  (fake delta) and produce new image  $\hat{Y}^S$ . To ensure that fake deltas function similarly to real ones, we introduce a novel adversarial delta matching loss by using a delta matching discriminator to judge whether an input-output image pair matches the corresponding delta. Besides, we employ a variant of mode seeking loss [24] to alleviate the mode collapse issue. We also employ typical adversarial loss and classification loss to make the generated images realistic and category-preserving. In the testing stage, given a conditional unseen image  $X^U$ , we can obtain its sample-specific deltas by sampling random vectors as shown in Figure 2(b). Because each delta represents one possible intra-category transformation, given a conditional unseen image, different deltas can produce realistic and diverse images from the same unseen category. Extensive experiments on six benchmark datasets demonstrate the effectiveness of our proposed method. Our contributions can be summarized as follows:

- We propose a novel delta-based few-shot image generation method, which has never been explored before.
- Technically, we extend few-shot feature generation method Delta-encoder to few-shot image generation with stochastic sampling and sample-specific delta. We also design a novel adversarial delta matching loss.
- Our method can produce diverse and realistic images for each unseen category based on a single conditional image, surpassing existing few-shot image generation methods by a large margin.

## II. RELATED WORK

**Data augmentation:** Data augmentation targets at augmenting training data with new samples. New samples obtained by traditional data augmentation tricks (*e.g.*, crop, flip, color jittering) only have limited diversity. Also, there are some methods such as AutoAugment [25], Fast-AutoAugment [26], PBA [27], and AWS [28] proposed to learn optimal augmentation strategies to

improve the accuracy of classifiers. Similarly, neural augmentation [29], [30], [31], [32], [33] allowed a network to learn augmentations that can improve the classifiers to the utmost. As another research line, deep generative models can generate more diverse samples to augment training data, which can be categorized into feature-based augmentation methods [19] and image-based augmentation methods [21]. Feature-based augmentation methods [34], [35] focused on generating more diverse deep features to augment the feature space of training data, while image-based augmentation methods [36], [37], [15], [16] targeted at exploiting the distribution of training images and generating more diverse images.

**Few-shot feature generation** In existing few-shot feature generation methods, the semantic knowledge learned from the seen categories is transferred to compensate unseen categories in [38], [35]. cCov-GAN [39] proposed a covariance-preserving adversarial augmentation network to generate more features for unseen categories. In [40], a generator subnetwork was added to a classification network to generate new examples. Intra-category diversity learned from seen categories was transferred to unseen categories to generate new features in [21], [41]. Dual TriNet [34] proposed to synthesize instance features by leveraging semantics using a novel auto-encoder network for unseen categories.

**Few-shot image generation** Compared with few-shot feature generation, few-shot image generation is a more challenging problem. Early methods can only be applied to generate new images for simple concepts, such as Bayesian program learning in [42], Bayesian reasoning in [43], and neural attention in [44]. Recently, several more advanced methods have been proposed to generate new real-world images in few-shot setting. To name a few, FIGR [14] (*resp.*, DAWSON [17]) combined adversarial learning with meta-learning method Reptile [45] (*resp.*, MAML [46]) to generate new images. GMN [18] (*resp.*, MatchingGAN [15]) combined meta-learning method Matching Network [47] with Variational Auto-Encoder [48] (*resp.*, Generative Adversarial Network [13]) to generate new images without finetuning in the test phase. F2GAN [16] was designed to enhance the fusion ability of model by filling the details borrowed from conditional images. Besides, DAGAN [19] proposed to produce new images by injecting random vectors into the generator conditioned on a single image. In this work, we propose a delta-based few-shot image generation method, which can produce more diverse images than previous methods based on a single image.

**Conditional image generation:** A wide range of conditional image generation applications have been inspired from conditional generative adversarial networks [49], such as image-to-image translation [50], [51], [52], super resolution [53], [54], [55], domain adaption [56], [10], single model image synthesis [57], [58], [59], style transfer [60], [61], image synthesis from text [62], [63], and so on. Most existing few-shot image generation methods including ours utilize conditional GAN for image generation, due to its remarkable performance. Compared with previous works [15], [18], [16] which are conditioned on multiple images, our DeltaGAN only depends on one conditional image, but can generate more realistic and diverse images.

### III. OUR METHOD

We split all categories into seen categories and unseen categories, which have no overlap. Our DeltaGAN mainly consists of a reconstruction subnetwork and a generation subnetwork as shown in Figure 3. The detailed architecture of each encoder/decoder is reported in Section IV-B. Given a same-category seen image pair  $\{x_1, x_2\}$  where  $x_1$  is the conditional image and  $x_2$  is the target image, the reconstruction subnetwork extracts real delta  $\Delta_{x_1}^r$  from this pair, and reconstructs the target image  $x_2$  based on  $x_1$  and  $\Delta_{x_1}^r$ . In the generation subnetwork, a random vector  $z$  and the conditional image  $x_1$  are used to obtain fake sample-specific delta  $\Delta_{x_1}^f$ , which collaborates with  $x_1$  to generate a new image  $\hat{x}_2$ . Moreover, we design an adversarial delta matching loss to bridge the gap between real delta and fake delta. Both reconstruction subnetwork and generation subnetwork are used in the training stage, while only generation subnetwork is used in the testing stage.

#### A. Reconstruction Subnetwork

In the reconstruction subnetwork, there are three encoders  $E_\Delta$ ,  $E_c$ ,  $E_r$  and a decoder  $G$ . Given a same-category seen image pair  $\{x_1, x_2\}$ , we use  $E_\Delta$  to extract paired features  $\{E_\Delta(x_1), E_\Delta(x_2)\} \in \mathcal{R}^{W \times H \times C}$ , where  $W \times H$  denotes the feature map size and  $C$  denotes the channel number. Then, we calculate the difference between  $E_\Delta(x_2)$  and  $E_\Delta(x_1)$ , which is fed into  $E_r$  to obtain real delta  $\Delta_{x_1}^r \in \mathcal{R}^{W \times H \times C}$ :

$$\Delta_{x_1}^r = E_r(E_\Delta(x_2) - E_\Delta(x_1)), \quad (1)$$

where  $\Delta_{x_1}^r$  contains the additional information needed to reconstruct  $x_2$  from  $x_1$ . We do not restrict our delta features to be linear offsets, which enables the delta features to learn more complex transformations. Then,  $\Delta_{x_1}^r$  is concatenated with  $E_c(x_1) \in \mathcal{R}^{W \times H \times C}$  and fed into  $G$  to obtain the reconstructed image  $\hat{x}_2$ :

$$\hat{x}_2 = G(\Delta_{x_1}^r, E_c(x_1)). \quad (2)$$

We employ a reconstruction loss  $\mathcal{L}_1$  to ensure that  $\hat{x}_2$  is close to  $x_2$ :

$$\mathcal{L}_1 = \|\hat{x}_2 - x_2\|_1. \quad (3)$$

Considering the instability issue of early training stage, we use a feature matching loss [64] by matching the discriminative feature of  $\hat{x}_2$  with that of  $x_2$ . In detail, we use a feature extractor  $\hat{D}_I$  to extract the discriminative features of  $\hat{x}_2$  and  $x_2$  in each layer to calculate the feature matching loss:

$$\mathcal{L}_{fm} = \frac{1}{L} \sum_{l=1}^L \|\hat{D}_I^l(x_2) - \hat{D}_I^l(\hat{x}_2)\|_1, \quad (4)$$

where  $L$  is the layer number of  $\hat{D}_I$ .

#### B. Generation Subnetwork

To support stochastic sampling for generation, we design another generation subnetwork in parallel with the reconstruction subnetwork. Two subnetworks share two encoders  $E_\Delta$ ,  $E_c$  and the decoder  $G$ . Besides, a new encoder  $E_f$  is introduced to obtain fake sample-specific delta. In our

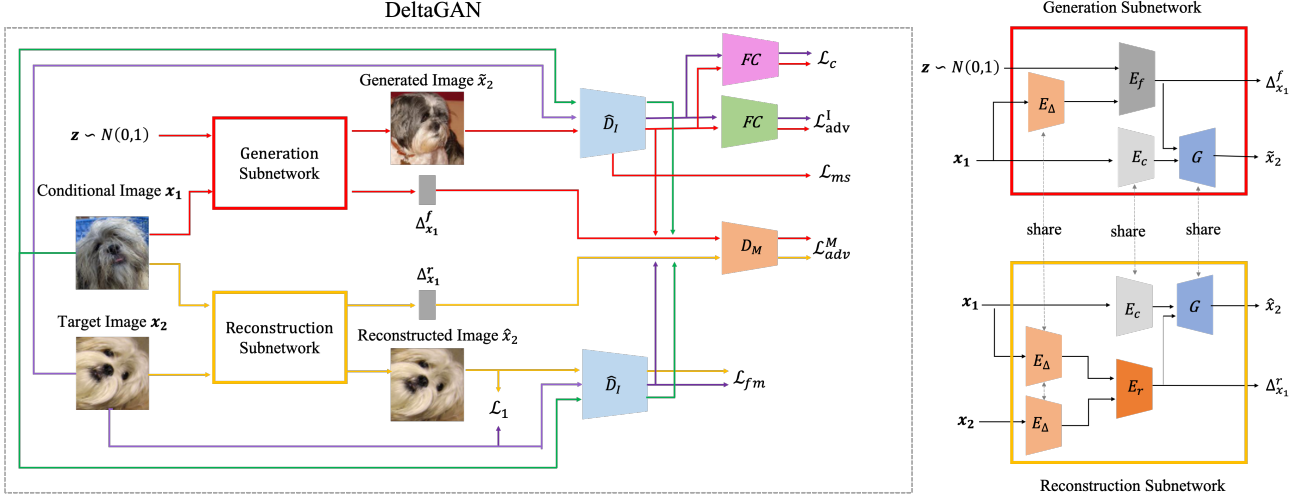


Figure 3: Our DeltaGAN mainly consists of a reconstruction subnetwork and a generation subnetwork. In the generation subnetwork,  $\tilde{x}_2$  is generated based on the random vector  $z$  and the conditional image  $x_1$ . In the reconstruction subnetwork, the target image  $x_2$  is reconstructed based on the conditional image  $x_1$  and the delta between  $x_1$  and  $x_2$ . Best viewed in color.

generation subnetwork, we concatenate a random vector  $z$  sampled from unit Gaussian distribution and the feature of conditional image  $E_\Delta(x_1) \in \mathcal{R}^{W \times H \times C}$ , which is fed into  $E_f$  to obtain sample-specific delta  $\Delta_{x_1}^f \in \mathcal{R}^{W \times H \times C}$ :

$$\Delta_{x_1}^f = E_f(z, E_\Delta(x_1)), \quad (5)$$

where  $\Delta_{x_1}^f$  contains the additional information needed to transform conditional image  $x_1$  to another possible image within the same category. Then, analogous to the reconstruction subnetwork,  $\Delta_{x_1}^f$  is concatenated with  $E_c(x_1)$  and fed into  $G$  to produce a new image  $\tilde{x}_2$  belonging to the category of  $x_1$ :

$$\tilde{x}_2 = G(\Delta_{x_1}^f, E_c(x_1)), \quad (6)$$

in which  $\tilde{x}_2$  is the transformed result after applying delta  $\Delta_{x_1}^f$  to  $x_1$ .

**Adversarial loss:** To make the generated image  $\tilde{x}_2$  close to real images, we employ a standard adversarial loss using the discriminator  $D_I$ .  $D_I$  contains the feature extractor  $\hat{D}_I$  mentioned in Section III-A and a fully-connected (FC) layer. We adopt the hinge adversarial loss proposed in [65]:

$$\begin{aligned} \mathcal{L}_{adv,D}^I &= \mathbb{E}_{x_2}[\max(0, 1 - D_I(x_2))] + \mathbb{E}_{\tilde{x}_2}[\max(0, 1 + D_I(\tilde{x}_2))], \\ \mathcal{L}_{adv,G}^I &= -\mathbb{E}_{\tilde{x}_2}[D_I(\tilde{x}_2)]. \end{aligned} \quad (7)$$

The discriminator  $D_I$  tends to distinguish fake images from real images by minimizing  $\mathcal{L}_{adv,D}^I$ , while the generator tends to generate realistic images to fool the discriminator by minimizing  $\mathcal{L}_{adv,G}^I$ .

**Classification loss:** To ensure that  $\tilde{x}_2$  belongs to the expected category, we construct a classifier by replacing the last FC layer of  $D_I$  with another FC layer (the number of outputs is the number of seen categories), analogous to ACGAN [66]. Then, the images from different categories can be distinguished by a cross-entropy classification loss:

$$\mathcal{L}_c = -\log p(c(x)|x), \quad (8)$$

where  $c(x)$  is the category label of  $x$ . We train the classifier by minimizing  $\mathcal{L}_{c,D} = -\log p(c(x_2)|x_2)$  of the target image  $x_2$ . We also expect the generated image  $\tilde{x}_2$  to be classified as the same category of target image  $x_2$ . Thus, we minimize  $\mathcal{L}_{c,G} = -\log p(c(x_2)|\tilde{x}_2)$  when updating the generator.

**Adversarial delta matching loss:** To ensure that the generated sample-specific deltas function similarly to real deltas and encode the intra-category transformation, we design a novel adversarial delta matching loss to bridge the gap between real deltas and fake deltas. This goal is accomplished by a delta matching discriminator  $D_M$ , which takes a triplet (conditional image, output image, the delta between them) as input. As shown in Figure 3, we extract the features of paired images  $\{\hat{D}_I(x_1), \hat{D}_I(x_2)\}$  (resp.,  $\{\hat{D}_I(x_1), \hat{D}_I(\tilde{x}_2)\}$ ), which are concatenated with sample-specific delta  $\Delta_{x_1}^r$  (resp.,  $\Delta_{x_1}^f$ ) to form a real (resp., fake) triplet. Then, the real triplet and fake triplet are fed into the delta matching discriminator  $D_M$  to judge whether this conditional-output image pair matches the corresponding delta, in other words, whether the delta is the additional information required to transform the conditional image to the output image. In adversarial learning, the discriminator needs to distinguish the real triplet  $\{\hat{D}_I(x_1), \hat{D}_I(x_2), \Delta_{x_1}^r\}$  from the fake triplet  $\{\hat{D}_I(x_1), \hat{D}_I(\tilde{x}_2), \Delta_{x_1}^f\}$ , while the generator aims to synthesize realistic fake triplet to fool the discriminator. The delta matching adversarial loss is also in the form of hinge adversarial loss [65], which can be written as

$$\begin{aligned} \mathcal{L}_{adv,D}^M &= \mathbb{E}_{x_1, x_2, \Delta_{x_1}^r}[\max(0, 1 - D_M(\hat{D}_I(x_1), \hat{D}_I(x_2), \Delta_{x_1}^r))] \\ &\quad + \mathbb{E}_{x_1, \tilde{x}_2, \Delta_{x_1}^f}[\max(0, 1 + D_M(\hat{D}_I(x_1), \hat{D}_I(\tilde{x}_2), \Delta_{x_1}^f))], \\ \mathcal{L}_{adv,G}^M &= -\mathbb{E}_{x_1, \tilde{x}_2, \Delta_{x_1}^f}[D_M(\hat{D}_I(x_1), \hat{D}_I(\tilde{x}_2), \Delta_{x_1}^f)], \end{aligned} \quad (9)$$

where  $\mathcal{L}_{adv,D}^M$  (resp.,  $\mathcal{L}_{adv,G}^M$ ) is optimized for updating  $\{\hat{D}_I, D_M\}$  (resp., the generator).

**Mode seeking loss:** We observe that by varying random vector  $z$ , the generated images may collapse into a few modes,



which is referred to as mode collapse [24]. Therefore, we use a variant of mode seeking loss [24] to seek for more modes to enhance the diversity of generated images. Different from [24], we apply mode seeking loss to multi-layer features extracted by  $\hat{D}_I$ . In particular, we minimize the ratio of the distance between  $z_1$  and  $z_2$  over the distance between  $\hat{D}_I^l(\tilde{x}_2^1)$  and  $\hat{D}_I^l(\tilde{x}_2^2)$  at the  $l$ -th layer of  $\hat{D}_I$ :

$$\mathcal{L}_{ms} = \frac{1}{L} \sum_{l=1}^L \frac{\|z_1 - z_2\|_1}{\|\hat{D}_I^l(\tilde{x}_2^1) - \hat{D}_I^l(\tilde{x}_2^2)\|_1}. \quad (10)$$

Intuitively, when  $\|z_1 - z_2\|_1$  is large, we expect  $\hat{D}_I^l(\tilde{x}_2^1)$  and  $\hat{D}_I^l(\tilde{x}_2^2)$  to be considerably different, which can push the generator to search more modes to produce diverse images. In our experiments (see Section IV-H), we find that mode seeking loss is critical for diversity. However, without the guidance of reconstruction subnetwork and adversarial delta matching loss, solely using mode seeking loss cannot generate meaningful deltas, with both diversity and realism significantly downgraded.

### C. Optimization

We use  $\theta_G$  to denote the model parameters of  $\{E_\Delta, E_r, E_c, E_f, G\}$ , while  $\theta_D$  is used to denote the model parameters of  $\{D_I, D_M\}$ . The total loss function of our method can be written as

$$\mathcal{L} = \mathcal{L}_{adv}^I + \mathcal{L}_{adv}^M + \lambda_1 \mathcal{L}_1 + \mathcal{L}_c + \lambda_{fm} \mathcal{L}_{fm} + \lambda_{ms} \mathcal{L}_{ms}, \quad (11)$$

in which  $\lambda_1$ ,  $\lambda_{fm}$ , and  $\lambda_{ms}$  are trade-off parameters.  $\mathcal{L}_{adv}^I$  represents  $\mathcal{L}_{adv,G}^I$  (*resp.*,  $\mathcal{L}_{adv,D}^I$ ) when updating the model parameters  $\theta_G$  (*resp.*,  $\theta_D$ ). Similarly,  $\mathcal{L}_{adv}^M$  represents  $\mathcal{L}_{adv,G}^M$  (*resp.*,  $\mathcal{L}_{adv,D}^M$ ) when updating the model parameters  $\theta_G$  (*resp.*,  $\theta_D$ ).

$\theta_G$  and  $\theta_D$  are optimized using related loss terms in an alternating fashion. In particular,  $\theta_D$  is optimized by minimizing  $\mathcal{L}_{adv,D}^I + \mathcal{L}_{adv,D}^M + \mathcal{L}_{c,D}$  similar to ACGAN [66].  $\theta_G$  is optimized by minimizing  $\mathcal{L}_{adv,G}^I + \mathcal{L}_{adv,G}^M + \lambda_1 \mathcal{L}_1 + \mathcal{L}_{c,G} + \lambda_{fm} \mathcal{L}_{fm} + \lambda_{ms} \mathcal{L}_{ms}$ , in which  $\mathcal{L}_{c,D}$  and  $\mathcal{L}_{c,G}$  are defined below Eqn. (8).

## IV. EXPERIMENTS

### A. Datasets and Implementation Details

We conduct experiments on six few-shot image datasets: EMNIST [67], VGGFace [68], Flowers [69], Animal Faces [70], NABirds [71], and Foods [72]. Following the split setting of MatchingGAN [15] (*resp.*, FUNIT [50]), we split VGGFace and EMNIST (*resp.*, Animal Faces, Flowers, NABirds, and Foods) into seen categories and unseen categories. In detail, for VGGFace (*resp.*, EMNIST) dataset, we randomly select 1802 (*resp.*, 28) categories from all categories as seen training categories and select 96 (*resp.*, 10) categories from remaining categories as unseen testing categories. On Flowers (*resp.*, Animal Faces, NABirds, and Foods) dataset, a total of 102 (*resp.*, 149, 555, and 256) categories are split into 85 (*resp.*, 119, 444, and 224) seen categories and 17 (*resp.*, 30, 111, and 32) unseen categories. In Table I, we summarize the number of seen/unseen categories and the number of seen/unseen images.

Table I: The splits of seen/unseen images (“img”) and categories (“cat”) on six datasets.

Dataset	Seen		Unseen	
	#img	#cat	#img	#cat
EMNIST [67]	78400	28	28000	10
VGGFace [68]	180200	1802	9600	96
Flowers [69]	7121	85	1068	17
Animal Faces [70]	96621	119	20863	30
NABirds [71]	38306	444	10221	111
Foods [72]	27471	224	3924	32

Table II: The number of model parameters of MatchingGAN [15], F2GAN [16], and our DeltaGAN.

Setting	Training phase	Testing phase
MatchingGAN [15]	30.3M	9.8M
F2GAN [16]	31.1M	9.9M
DeltaGAN	33.1M	8.1M

After having a few trials, we set  $\lambda_1 = 10$ ,  $\lambda_{fm} = 0.1$ , and  $\lambda_{ms} = 10$  by observing the quality of generated images during training. We implement our model using the TensorFlow 1.13.1 environment on Ubuntu 16.04 LTS equipped by GEFORCE RTX 2080 Ti GPU and Intel(R) Xeon(R) CPU E5 – 2660 v3 @ 2.60GHz CPU. We adopt Adam optimizer with an initial learning rate of 0.0001. The batch size is set to 16 and our model is trained for 200 epochs.

### B. Details of Network Architecture

**Generator** Our generator consists of a reconstruction subnetwork and a generation subnetwork. Our reconstruction subnetwork (*resp.*, generation subnetwork) is constructed by 3 encoders including  $E_\Delta$ ,  $E_c$ , and  $E_r$  (*resp.*,  $E_f$ ) and 1 decoder  $G$ . Encoder  $E_\Delta$  has 5 residual blocks (ResBlks), which consists of 4 encoder blocks and 1 intermediate block. Each encoder block contains 3 convolutional layers with leaky ReLU and batch normalization followed by one downsampling layer, while the intermediate block contains 3 convolutional layers with leaky ReLU and batch normalization. The structure of encoder  $E_c$  is the same as encoder  $E_\Delta$  without parameters sharing. Encoder  $E_r$  consists of two Conv-LRelu-BN blocks, in which each block contains 1 convolutional layer with leaky ReLU and batch normalization. Encoder  $E_f$  also has two Conv-LRelu-BN blocks. The decoder  $G$  consists of 4 residual blocks (ResBlks), in which each block contains 3 convolutional layers with leaky ReLU and batch normalization followed by one upsampling layer.

**Discriminator** Our discriminator  $D_I$  is analogous to that in [50], which consists of one convolutional layer followed by four groups of ResBlk. Each group of ResBlk is as follows:  $\text{ResBlk-}k \rightarrow \text{ResBlk-}k \rightarrow \text{AvePool2x2}$ , where  $\text{ResBlk-}k$  is a ReLU first residual block [73] with the number of channels  $k$  set as 64, 128, 256, 512 in four groups. We use one fully connected (FC) layer with 1 output following global average pooling (GAP) to obtain the discriminator score. Our discriminator  $D_M$  is constructed by four FC layers following GAP. The classifier shares the feature extractor with the discriminator  $D_I$  and only replaces the last FC layer with

another FC layer with the number of outputs being the number of seen categories.

**The number of model parameters** We compare the number of model parameters of our DeltaGAN with MatchingGAN [15] and F2GAN [16] in the training stage and testing stage, respectively. In the training stage, The model parameters of generator and discriminator are trainable to complete two-player adversarial learning with seen categories, while only generator is used to generate new images for each unseen category in the testing stage. In particular, our DeltaGAN only uses generation subnetwork to generate new images without reconstruction subnetwork. In Table II, we can see that our DeltaGAN uses fewer model parameters to generate images of better quality compared with MatchingGAN and F2GAN in the testing stage.

### C. Evaluation of Generated Images

To evaluate the quality of images generated by different methods, we calculate Fréchet Inception Distance (FID) [81] and Learned Perceptual Image Patch Similarity (LPIPS) [82] on four datasets. FID is used to measure the distance between generated unseen images and real unseen images. We remove the last average pooling layer of the ImageNet-pretrained Inception-V3 model and use the remaining network as the feature extractor. Then, we calculate FID between the extracted features of generated unseen images and those of real unseen images. LPIPS is used to measure the diversity of generated unseen images. For each unseen category, the average of pairwise distances among generated images is calculated, and then the average of all unseen categories is calculated as the final LPIPS score.

Since the number of conditional images in fusion-based methods GMN [18], MatchingGAN [15], and F2GAN [16] is a tunable hyper-parameter, we follow F2GAN [16] to use 3 conditional images in each training and testing episode. In the testing stage, if  $K$  images are provided for each unseen category, we refer to this setting as  $K$ -shot setting. We report the 3-shot results for all methods and 1-shot results for the methods which only require one conditional image. In either setting, following [15], [16], we use each method to generate 128 images for each unseen category, which are used to calculate FID and LPIPS. For DeltaGAN and DAGAN which are applicable to both 1-shot and 3-shot settings, we generate 128 images based on one conditional image in 1-shot setting and generate 128 images by randomly sampling one conditional image each time in 3-shot setting.

The results are summarized in Table III, we can observe that our method achieves the lowest FID and highest LPIPS in the 3-shot setting, which demonstrates that our method could generate more diverse and realistic images compared with baseline methods. Besides, our method in 1-shot setting also achieves competitive results, which are even better than other baselines in 3-shot setting.

We show some example images generated by our DeltaGAN on six datasets in Figure 4. We exhibit 12 generated images based on one conditional unseen image by sampling different random vectors. On EMNIST dataset, we can see that generated images maintain the concepts of conditional images and

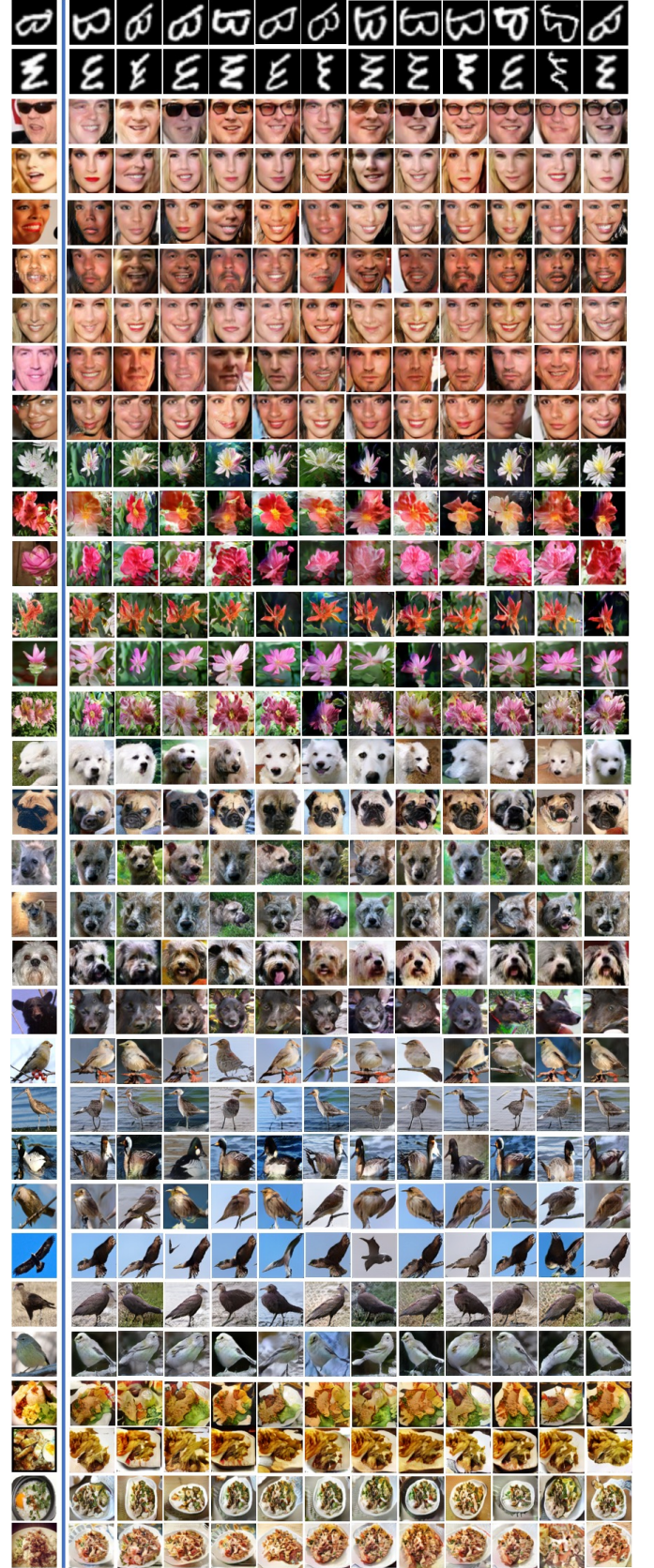


Figure 4: Images generated by our DeltaGAN in 1-shot setting on six datasets (from top to bottom: EMNIST, VGGFace, Flowers, Animal Faces, NABirds, and Foods). The conditional images are in the leftmost column.



Table III: FID ( $\downarrow$ ) and LPIPS ( $\uparrow$ ) of images generated by different methods for unseen categories on four datasets (from left to right: VGGFace, Flowers, Animal Faces, and NABirds).

Method	Setting	VGGFace		Flowers		Animal Faces		NABirds	
		FID ( $\downarrow$ )	LPIPS( $\uparrow$ )	FID ( $\downarrow$ )	LPIPS ( $\uparrow$ )	FID ( $\downarrow$ )	LPIPS ( $\uparrow$ )	FID ( $\downarrow$ )	LPIPS ( $\uparrow$ )
FIGR [14]	3-shot	139.83	0.0834	190.12	0.0634	211.54	0.0756	210.75	0.0918
GMN [18]	3-shot	136.21	0.0902	200.11	0.0743	220.45	0.0868	208.74	0.0923
DAWSON [17]	3-shot	137.82	0.0769	188.96	0.0583	208.68	0.0642	181.97	0.1105
DAGAN [19]	3-shot	128.34	0.0913	151.21	0.0812	155.29	0.0892	159.69	0.1405
DAGAN [19]	1-shot	134.28	0.0608	179.59	0.0496	185.54	0.0687	183.57	0.0967
MatchingGAN [15]	3-shot	118.62	0.1695	143.35	0.1627	148.52	0.1514	142.52	0.1915
F2GAN [16]	3-shot	109.16	0.2125	120.48	0.2172	117.74	0.1831	126.15	0.2015
DeltaGAN	3-shot	<b>78.35</b>	<b>0.3487</b>	<b>104.62</b>	<b>0.4281</b>	<b>87.04</b>	<b>0.4642</b>	<b>95.97</b>	<b>0.5136</b>
DeltaGAN	1-shot	<b>80.12</b>	<b>0.3146</b>	<b>109.78</b>	<b>0.3912</b>	<b>89.81</b>	<b>0.4418</b>	<b>96.79</b>	<b>0.5069</b>

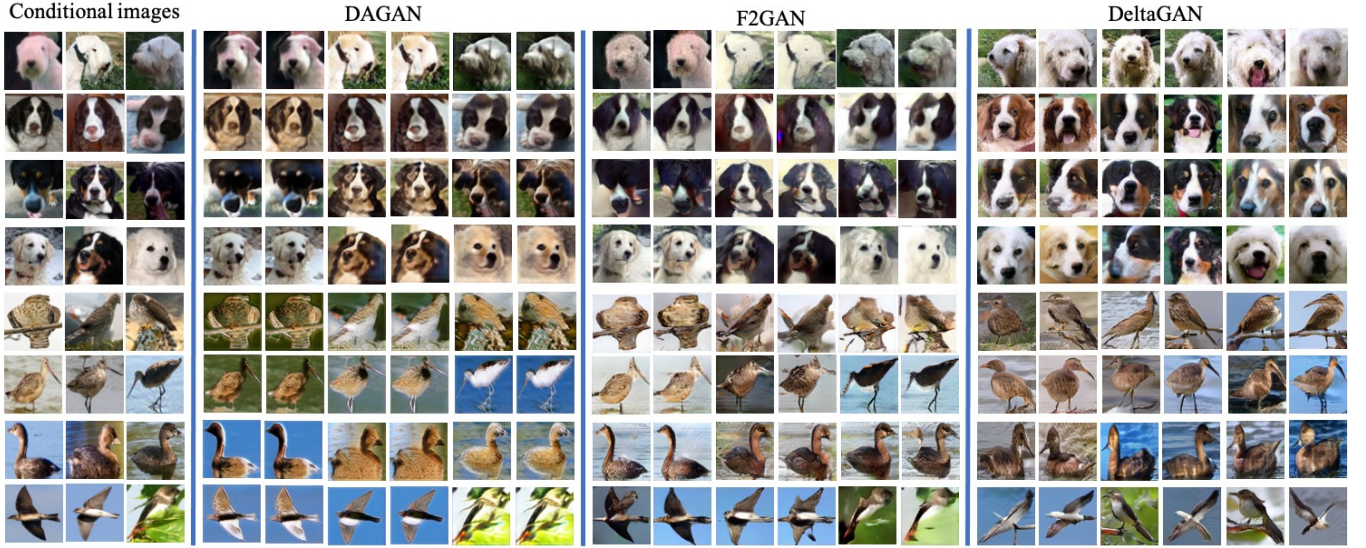


Figure 5: Images generated by DAGAN [19], F2GAN [16], and our DeltaGAN in 3-shot setting on two datasets (from top to bottom: Animal Faces and NABirds). The conditional images are in the left three columns.

have remarkable diversity. On natural datasets VGGFace, Flowers, Animal Faces, NABirds, and Foods, our DeltaGAN can generate diverse images with high fidelity.

For comparison, we also show some example images generated by DAGAN and F2GAN in Figure 5. For DAGAN, we arrange the results according to the conditional image. It can be seen that the structures of images produced by DAGAN are almost the same as the conditional image. For F2GAN, the generated images are still close to one of the conditional images and may have unreasonable shapes when fusing conditional images. Apparently, our DeltaGAN can produce images of higher quality and more diversity.

#### D. Few-shot Classification

In this section, we demonstrate that the new images generated by our DeltaGAN can greatly benefit few-shot classification. Following the  $N$ -way  $C$ -shot setting in few-shot classification [47], [74], in which evaluation episodes are created and the averaged accuracy over multiple evaluation episodes is calculated for evaluation. In each evaluation episode,  $N$  categories from unseen categories are randomly selected and  $C$  images from each of  $N$  categories are randomly selected.

These selected  $N \times C$  images are used as training set while the remaining unseen images from  $N$  unseen categories are used as test set. We pretrain ResNet18 [83] on the seen images and remove the last FC layer as the feature extractor, which is used to extract features for unseen images. In each evaluation episode in  $N$ -way  $C$ -shot setting, our DeltaGAN generates 512 new images to augment each of  $N$  categories. Based on the extracted features, we train a linear classifier with  $N \times (C+512)$  training images, which is then applied to the test set.

We compare our DeltaGAN with existing few-shot classification methods, including the representative methods MatchingNets [47], RelationNets [74], MAML [46] as well as the state-of-the-art methods MTL [75], DN4 [76], MatchingNet-LFT [77], DPGN [78], DeepEMD [79], and BSNet [80]. For these baselines, no augmented images are added to the training set in each evaluation episode. Instead, the images from seen categories are used to train those few-shot classifiers by strictly following their original training procedure. MAML [46] and MTL [75] models need to be finetuned based on the training set in each evaluation episode.

We also compare our DeltaGAN with few-shot image generation methods MatchingGAN [15] and F2GAN [16] as well

Table IV: Accuracy(%) of different methods on three datasets in few-shot classification setting. Note that fusion-based methods MatchingGAN [15] and F2GAN [16] are not applicable in 1-shot setting.

Method	VGGFace		Flowers		Animal Faces	
	10-way 1-shot	10-way 5-shot	10-way 1-shot	10-way 5-shot	10-way 1-shot	10-way 5-shot
MatchingNets [47]	33.68	48.67	40.96	56.12	36.54	50.12
MAML [46]	32.16	47.89	42.95	58.01	35.98	49.89
RelationNets [74]	39.95	54.12	48.18	61.03	45.32	58.12
MTL [75]	51.45	68.95	54.34	73.24	52.54	70.91
DN4 [76]	52.88	70.02	56.76	73.96	53.26	71.34
MatchingNet-LFT [77]	54.34	69.92	58.41	74.32	56.83	71.62
DPGN [78]	54.83	70.27	58.95	74.56	57.18	72.02
Delta-encoder[21]	53.19	67.57	56.05	72.84	56.38	71.29
DeepEMD [79]	54.15	70.35	59.12	73.97	58.01	72.71
BSNet [80]	53.13	71.56	57.06	72.83	56.86	71.15
MatchingGAN [15]	-	70.94	-	74.09	-	70.89
F2GAN [16]	-	72.31	-	75.02	-	73.19
DeltaGAN	<b>56.85</b>	<b>75.71</b>	<b>61.23</b>	<b>77.09</b>	<b>60.31</b>	<b>74.59</b>

Table V: Accuracy(%) of different methods on two datasets in low-data setting. Among few-shot image generation methods, only DAGAN and our DeltaGAN are applicable in 1-sample setting.

Method	EMNIST				VGGFace			
	1-sample	5-sample	10-sample	15-sample	1-sample	5-sample	10-sample	15-sample
Standard	50.14	83.64	88.64	91.14	5.08	8.82	20.29	39.12
Traditional	52.82	84.62	89.63	92.07	8.87	9.12	22.83	41.63
FIGR [14]	-	85.91	90.08	92.18	-	6.12	18.84	32.13
GMN [18]	-	84.12	91.21	92.09	-	5.23	15.61	35.48
DAWSON [17]	-	83.63	90.72	91.83	-	5.27	16.92	30.61
DAGAN [19]	57.84	87.45	94.18	95.58	13.27	19.23	35.12	44.36
MatchingGAN [15]	-	91.75	95.91	96.29	-	21.12	40.95	50.12
F2GAN [16]	-	93.18	97.01	97.82	-	24.76	43.21	53.42
DeltaGAN	<b>84.56</b>	<b>96.02</b>	<b>98.12</b>	<b>98.87</b>	<b>22.91</b>	<b>28.91</b>	<b>50.19</b>	<b>58.72</b>

as few-shot feature generation method Delta-encoder [21]. We adopt the same augmentation strategy as our DeltaGAN in each evaluation episode. Besides, we compare our DeltaGAN with few-shot image translation method FUNIT [50] in Section IV-J.

By taking 10-way 1-shot/5-shot as examples, we report the averaged accuracy over 10 episodes on three datasets in Table IV. Our method achieves the best performance on all datasets compared with few-shot classification and few-shot generation baselines, which demonstrates the high quality of generated images by our DeltaGAN.

### E. Low-data Classification

To further evaluate the quality of our generated images, we conduct downstream classification tasks in low-data setting by using generated images to augment unseen categories. Following F2GAN [16], for each unseen category, we randomly select a few (*e.g.*,  $K = 1, 5, 10, 15$ ) training images and use the remaining images as test images, which is referred to as  $K$ -sample in Table V. We initialize ResNet18 [83] backbone based on seen categories, then finetune the whole network with the training images of unseen categories, and finally apply the trained classifier to the test images of unseen categories. This setting is referred to as “Standard” in Table V.

Then, we augment unseen training images with new images generated by different few-shot image generation methods. For each unseen category, one method generates 512 images by randomly sampling conditional images from the training set of this unseen category. Then, we augment the original training set

of unseen categories with generated images, which are used to finetune the ResNet18 classifier. In addition, we compare with traditional data augmentation (*e.g.*, flip, crop, color jittering), which also generates 512 new images for each unseen category. The setting of traditional data augmentation is referred to as “Traditional” in Table V. The results of different methods are reported in Table V. We can see that our DeltaGAN achieves better results than traditional data augmentation methods as well as few-shot image generation baselines, which shows the effectiveness of using augmented images produced by our DeltaGAN for low-shot classification task.

### F. Delta Interpolation

To evaluate whether the delta space of DeltaGAN is densely populated, we perform linear interpolation based on two random vectors  $z_1$  and  $z_2$ . In detail, we calculate the interpolated random vector  $z = a_1 z_1 + a_2 z_2$  ( $a_1 + a_2 = 1$ ) by gradually decreasing (*resp.*, increasing)  $a_1$  (*resp.*,  $a_2$ ) from 1 (*resp.*, 0) to 0 (*resp.*, 1) with step size 0.1. We use one conditional image and interpolated  $z$  to generate sample-specific deltas, which are used to produce interpolation results in Figure 6. We can see that our DeltaGAN can generate diverse images with smooth transition between two random vectors  $z_1$  and  $z_2$ , including the transition between different colors, shapes, and poses.

### G. Image Reconstruction Results

In the training stage, our reconstruction network can reconstruct  $x_2$  based on  $x_1$  and  $\Delta_{x_1}^r$ . To demonstrate that

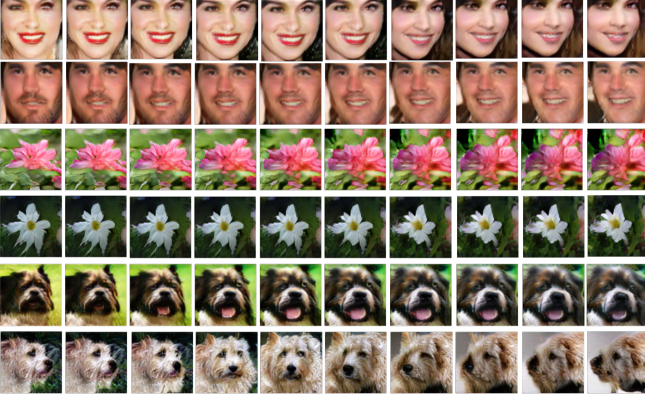


Figure 6: Images generated by our DeltaGAN by interpolating random vectors between  $z_1$  and  $z_2$  on three datasets (from top to bottom: VGGFace, Flowers, and Animal Faces).

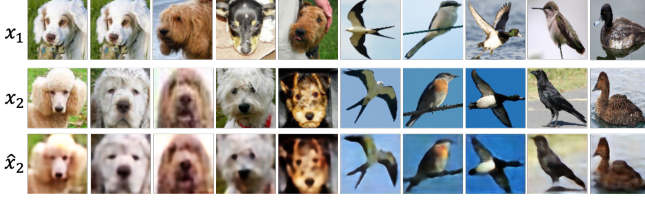


Figure 7: Reconstruction results of our DeltaGAN on Animal Faces (left) and NABirds (right) datasets. The conditional images  $x_1$  are in the first row, the target images  $x_2$  are in the second row, and the reconstructed images  $\hat{x}_2$  are in the third row.

the reconstruction ability of reconstruction subnetwork can be transferred from seen categories to unseen categories, we visualize the reconstructed unseen images on Animal Faces and NABirds datasets in Figure 7. To be exact, we randomly sample same-category unseen image pairs  $\{x_1, x_2\}$ , which pass through our reconstruction network to yield  $\hat{x}_2$ . From Figure 7, we can see that the reconstructed images  $\hat{x}_2$  are quite close to the target images  $x_2$ .

#### H. Ablation Studies

In this section, we analyze the impact of each loss term and alternative network designs on Animal Faces dataset. For all special cases of our method, we evaluate the quality of generated images from two aspects. On one hand, FID and LPIPS of generated images are computed in 1-shot setting as in Section IV-C. On the other hand, we report the accuracy of few-shot classification (10-way 1-shot) augmented with generated images as in Section IV-D.

**Loss terms:** In our method, we employ a reconstruction loss  $\mathcal{L}_1$  in Eqn. 3, a mode seeking loss  $\mathcal{L}_{ms}$  in Eqn. 10, a feature matching loss  $\mathcal{L}_{fm}$  in Eqn. 4, a classification loss  $\mathcal{L}_c$  in Eqn. 8, an adversarial loss  $\{\mathcal{L}_{adv,D}^I, \mathcal{L}_{adv,G}^I\}$  in Eqn. 7, and an adversarial delta matching loss  $\{\mathcal{L}_{adv,D}^M, \mathcal{L}_{adv,G}^M\}$  in Eqn. 9. To investigate the impact of each loss term, we conduct ablation studies on Animal Faces dataset by removing each loss term from the final objective in Eqn. 11 separately. The results are

Table VI: Ablation studies of our loss terms and alternative network designs on Animal Faces dataset.

Setting	Accuracy(%) $\uparrow$	FID $\downarrow$	LPIPS $\uparrow$
w/o $\mathcal{L}_1$	58.68	100.21	0.4191
w/o $\mathcal{L}_{ms}$	50.08	121.74	0.2976
w/o $\mathcal{L}_{fm}$	59.17	95.82	0.4324
w/o $\mathcal{L}_c$	42.21	196.18	0.4119
w/o $\mathcal{L}_{adv,D}^I$	52.18	139.46	0.3912
w/o $\mathcal{L}_{adv,G}^I$	57.12	115.11	0.4153
w/o real delta	53.03	128.69	0.3838
Prior delta	46.25	208.31	0.2431
Global delta	58.96	94.51	0.4311
SC delta	56.11	101.05	0.4162
DC delta	55.29	105.91	0.4021
Simple $D_1$	54.53	129.17	0.3012
Simple $D_2$	58.01	109.54	0.4401
Simple $D_3$	59.51	94.12	0.4392
Linear delta	53.89	122.71	0.4091
DeltaGAN	<b>60.31</b>	<b>89.81</b>	<b>0.4418</b>

summarized in Table VI, which shows that the diversity and fidelity of generated images are compromised when removing  $\mathcal{L}_1$ . By removing mode seeking loss  $\mathcal{L}_{ms}$ , we can see that all metrics become much worse, which implies the mode collapse issue after removing  $\mathcal{L}_{ms}$ . Another observation is that ablating  $\mathcal{L}_{fm}$  leads to slight degradation of generated images. Removing  $\mathcal{L}_c$  results in severe degradation of generated images, since the generated images may not belong to the category of conditional image. When  $\{\mathcal{L}_{adv,D}^I, \mathcal{L}_{adv,G}^I\}$  is removed from the final objective, the worse quality of generated images indicates that typical adversarial loss can ensure the fidelity of generated images. Without considering the gap between real delta and fake delta by removing  $\{\mathcal{L}_{adv,D}^M, \mathcal{L}_{adv,G}^M\}$ , it can be seen that the quality of generated images becomes worse.

**Without real delta:** To investigate the necessity of enforcing generated fake deltas to be close to real deltas, we cut off the links between real delta and fake delta by removing the reconstruction subnetwork and adversarial delta matching loss (i.e., removing  $\{\mathcal{L}_{adv,D}^M, \mathcal{L}_{adv,G}^M, \mathcal{L}_1, \mathcal{L}_{fm}\}$ ), which is referred to as “w/o real delta”. Compared with DeltaGAN, both diversity and realism are significantly degraded, because generation subnetwork fails to generate meaningful deltas without the guidance of reconstruction subnetwork and adversarial delta matching loss. Thus, we conclude that mode seeking loss needs to cooperate with our framework to produce realistic and diverse images.

Another observation is that “w/o  $\mathcal{L}_{adv}^M$ ” is better than “w/o real delta”, which can be explained as follows. Even without using adversarial delta matching loss, since the reconstruction subnetwork and the generation subnetwork share the same  $E_c$  and  $G$ , generated fake deltas have been implicitly pulled close to real deltas.

**Sample-specific delta:** As mentioned in Section I, one simple modification of Figure 1(a) to support stochastic sampling is enforcing the extracted deltas to follow a prior distribution (e.g., unit Gaussian distribution) with KL divergence loss, so that we can sample random vectors from the prior distribution to generate new images in the testing stage. We report the results of this modification as “Prior delta” in Table VI, which shows that it is difficult to generate high-quality diverse images





Figure 8: Visualization results of exchanging delta in the reconstruction subnetwork on Animal Faces. From top to bottom: conditional image  $x_1$ , a pair of  $x_2$  and  $x_3$  providing real delta,  $\tilde{x}$  generated based on  $x_1$  and the real delta.



Figure 9: Visualization results of exchanging delta in the generation subnetwork on Animal Faces. From top to bottom: conditional image  $x_1$ ,  $x_2$  providing the delta,  $\tilde{x}$  generated based on  $x_1$  and the delta of  $x_2$ .

by enforcing the extracted deltas to follow a prior distribution.

To corroborate the superiority of sample-specific delta, we directly use random vectors to generate deltas as shown in Figure 1(b), which is referred to as “Global delta” in Table VI. It can be seen that our design of sample-specific deltas can benefit the quality of generated images.

Besides, with our trained DeltaGAN model, we explore some different image generation strategies. Specifically, we exchange sample-specific deltas within images from the same category to generate new images, which is referred to as “SC delta” in Table VI. We also exchange sample-specific deltas within images across different categories, which is referred to as “DC delta” in Table VI. Compared with “SC delta” and “DC delta”, our DeltaGAN achieves the best performance on all metrics, which verifies our assumption that delta is sample-specific and exchangeable use of deltas may lead to performance drop.

**Delta matching discriminator:** As mentioned in Section III-B, we use conditional image, sample-specific delta, and output image as input triplet  $\{\hat{D}_I(x_1), \Delta_{x_1}, \hat{D}_I(x_2)\}$  for our delta matching discriminator  $D_M$ , which judges whether the conditional-output image pair matches the corresponding sample-specific delta. To evaluate the effectiveness and necessity of this input format, we explore different types of inputs for delta matching discriminator. As shown in Table VI, we use  $\{\Delta_{x_1}\}$  (resp.,  $\{\hat{D}_I(x_1), \Delta_{x_1}\}$ ,  $\{\hat{D}_I(x_2), \Delta_{x_1}\}$ ) as inputs of  $D_M$ , which is referred to as “Simple  $D_1$ ” (resp., “Simple  $D_2$ ”, “Simple  $D_3$ ”). We can see that “Simple  $D_1$ ” is the worst, which demonstrates that only employing adversarial loss on

delta does not work well. Besides, both “Simple  $D_2$ ” and “Simple  $D_3$ ” are worse than our DeltaGAN, which demonstrates the effectiveness of matching conditional-output image pair with the corresponding sample-specific delta.

**Linear offset delta:** To evaluate the effect of the learned non-linear “delta”, we replace the non-linear “delta” with linear “delta”, which is referred to as “Linear delta” in Table VI. In the reconstruction subnetwork, we set  $\Delta_{x_1}^r = E_\Delta(x_2) - E_\Delta(x_1)$ , and  $\hat{x}_2 = G(\Delta_{x_1}^r + E_c(x_1))$ , which means that we simply learn linear offset “delta” from same-class pairs of training data. In the generation subnetwork, we apply the generated fake “delta”  $\Delta_{x_1}^f$  to conditional image  $x_1$  to generate new image  $\tilde{x}_2 = G(\Delta_{x_1}^f + E_c(x_1))$ . Based on Table VI, the FID gap between “Linear delta” and “DeltaGAN” indicates that complex transformations of intra-category pairs cannot be well captured by linear offset.

### I. Visualization of Exchanging Delta

Note that our learnt delta is sample-specific delta. To check whether the delta is transferable across different images, we first show some generated images after exchanging delta in the reconstruction subnetwork. As shown in Figure 8, we extract real delta  $\Delta_{23}^r$  from one pair of images  $\{x_2, x_3\}$  from the same category as  $x_1$ , after which  $\Delta_{23}^r$  is applied to the conditional image  $x_1$  to generate a new image  $\tilde{x}$ . In column 1-2, we investigate a special case  $x_2 = x_3$ . In this case, the delta is vacuous and thus the generated image is close to the conditional image  $x_1$ . Recall that the real delta  $\Delta_{23}^r$  between  $x_2$  and  $x_3$  contains the necessary information required to transform  $x_2$  to  $x_3$ . In column 3-6, we show some cases, in which the delta appearance information or delta pose information encoded in  $\Delta_{23}^r$  influences  $x_1$  to some degree. For example, in column 3, the fur color of  $x_3$  is lighter than  $x_2$ , so the fur color of generated image  $\tilde{x}$  is also lighter than  $x_1$ . In Column 5,  $x_3$  turns face to the left compared with  $x_2$ , so  $\tilde{x}$  also turns face to the left compared with  $x_1$ . However, the generated images are generally of low quality. In column 7-8, the generated images  $\tilde{x}$  are corrupted when there is huge difference between  $x_2$  and  $x_3$  in appearance and pose.

Additionally, we show the visualization results of exchanging delta in the generation subnetwork in Figure 9, in which we apply the delta provided by  $x_2$  to the conditional image  $x_1$  to generate a new image  $\tilde{x}$ . The left (resp., right) four columns correspond to “SC delta” (resp., “DC delta”) in Table VI, in which  $x_2$  is from the same (resp., different) category of  $x_1$ . We can see that exchanging delta usually leads to severely degraded quality of generated images compared with DeltaGAN. Another observation is that “DC delta” is more inclined to generated unreasonable images compared with “SC delta”. These observations coincide with the quantitative results of “DC delta” and “SC delta” in Table VI.

As shown in Figure 8 and Figure 9, a plausible delta for one conditional image may be unsuitable for another conditional image, so we target at learning sample-specific delta. The learnt sample-specific delta has weak transferability across images and weaker transferability across categories. Hence, it is not suggested to generate new images by exchangeably

Table VII: Accuracy(%) of different methods on Animal Faces in few-shot classification setting. Note that MatchingGAN and F2GAN are not applicable in 1-shot setting.

Method	10-way 1-shot	10-way 5-shot
DPGN [78]	57.18	72.02
DeepEMD [79]	58.01	72.71
MatchingGAN [15]	-	70.89
F2GAN [16]	-	73.19
FUNIT-1	56.61	69.12
FUNIT-2	53.38	67.87
DeltaGAN	<b>60.31</b>	<b>74.59</b>

applying delta. However, the ability of generating effective sample-specific delta is transferable from seen categories to unseen categories, so our DeltaGAN is effective in producing new realistic images based on a conditional unseen image.

### J. Comparison with Few-shot Image Translation

Recently, few-shot image translation methods like FUNIT [50] have been proposed to translate seen images to unseen categories, which can also generate new images for unseen categories given a few images. However, the motivations of few-shot image generation and few-shot image translation are considerably different. Specifically, the former can generate new unseen images without touching seen images, while the latter relies on seen images to generate new unseen images. In particular, FUNIT disentangles the latent representation of an image into category-relevant representation (*i.e.*, class code) and category-irrelevant representation (*i.e.*, content code), in which appearance belongs to class code and pose belongs to content code [50]. In the testing stage, given a few images from one unseen category, FUNIT generates new images for this unseen category by combining the content codes of seen images with the class codes of these unseen images. However, in reality, the disentanglement in FUNIT is not perfect and the content code may also contain appearance information. So when translating seen images to unseen categories, the appearance information of seen images may be leaked to the generated new images. To corroborate this point, we visualize some example images generated by FUNIT. As shown in Figure 10, in column 1-4, the generated new images contain the appearance of seen images, which is against our expectation that the generated new images should be from unseen categories. In column 5-8, the generated images are even corrupted, probably due to incompatible content codes and class codes.

We also compare our DeltaGAN with FUNIT quantitatively for few-shot classification. By using the released model of FUNIT [50] trained on Animal Faces [70], we combine the content codes of seen images and the class codes of unseen images to produce 512 new images for each unseen category. Then, the generated images are used to facilitate few-shot classification, which is recorded as “FUNIT-1” in Table VII. However, “FUNIT-1” leverages seen images, which are not used in our DeltaGAN when generating new unseen images. For fair comparison, we also exchange content codes within the images from the same unseen category to produce new images, which is recorded as “FUNIT-2” in Table VII. In this case, we can only generate  $(C - 1) \times C$  new images for each



Figure 10: Images generated by FUNIT [50] in 1-shot setting on Animal Faces. Unseen (*resp.*, seen) images are shown in the first (*resp.*, second) row. In each column, the new image is generated by combining the class code of unseen image and the content code of seen image.

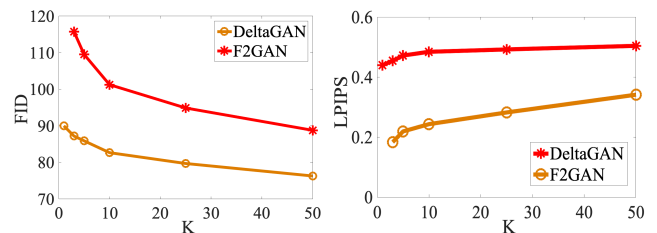


Figure 11: FID and LPIPS comparison between F2GAN and our DeltaGAN with different numbers ( $K$ ) of conditional images on Animal Faces.

unseen category in  $N$ -way  $C$ -shot setting. Based on Table VII, we observe that “FUNIT-2” is much worse than “FUNIT-1”, because “FUNIT-1” resorts to a large number of extra seen images to generate more unseen images than “FUNIT-2”. We also observe that “FUNIT-1” underperforms some few-shot classification methods and some few-shot image generation methods (*e.g.*, F2GAN, DeltaGAN), which may be attributed to the appearance information leakage or image corruption as shown in Figure 10.

### K. Few-shot Generation Ability

Here, we repeat the experiments in Section IV-C except tuning  $K$  in a wide range. Recall that  $K$  in  $K$ -shot setting means that  $K$  real images are provided for each unseen category. We use our DeltaGAN and competitive baseline F2GAN to generate 128 new images for each unseen category in  $K$ -shot setting. We also adopt the same quantitative evaluation metrics (FID and LPIPS) to measure image quality and diversity as in Section IV-C. We plot the FID curve and LPIPS curve of two methods with increasing  $K$  in Figure 11. It can be seen that our DeltaGAN outperforms F2GAN by a large margin with all values of  $K$ , especially when  $K$  is very small. These results demonstrate that our DeltaGAN can generate abundant diverse and realistic images even if only a few (*e.g.*, 10) real images are provided.

### L. Failure Case

We show some failure cases of our DeltaGAN on Animal Faces dataset in Figure 12. Due to the complexity of transformations between intra-category pairs, when applying the



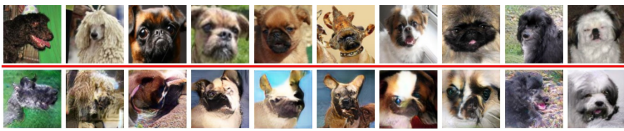


Figure 12: Failure cases of our DeltaGAN on Animal Faces dataset. The conditional images are shown in the top row and the generated images are shown in the bottom row.

generated deltas to the conditional images (top row), some deltas may generate distorted images (bottom row).

## V. CONCLUSION

In this paper, we have explored applying sample-specific deltas to a conditional image to generate new images. Specifically, we have proposed a novel few-shot generation method DeltaGAN composed of a reconstruction subnetwork and a generation subnetwork, which are bridged by an adversarial delta matching loss. The experimental results on six datasets have shown that our DeltaGAN can substantially improve the quality and diversity of generated images compared with existing few-shot image generation methods.

## REFERENCES

- [1] T. Karras, S. Laine, and T. Aila, "A style-based generator architecture for generative adversarial networks," in *Proceedings of Conference on Computer Vision and Pattern Recognition (CVPR)*, 2019.
- [2] T. Karras, S. Laine, M. Aittala, J. Hellsten, J. Lehtinen, and T. Aila, "Analyzing and improving the image quality of StyleGAN," *arXiv preprint arXiv:1912.04958*, 2019.
- [3] T. Karras, T. Aila, S. Laine, and J. Lehtinen, "Progressive growing of gans for improved quality, stability, and variation," in *Proceedings of International Conference on Learning Representations*, 2018.
- [4] M. Bińkowski, D. J. Sutherland, M. Arbel, and A. Gretton, "Demystifying MMD GANs," in *Proceedings of International Conference on Learning Representations*, 2018.
- [5] X. Mao, Q. Li, H. Xie, R. Y. Lau, Z. Wang, and S. Paul Smolley, "Least squares generative adversarial networks," in *Proceedings of international conference on computer vision*, 2017.
- [6] T. Miyato, T. Kataoka, M. Koyama, and Y. Yoshida, "Spectral normalization for generative adversarial networks," in *Proceedings of 6th International Conference on Learning Representations (ICLR)*, 2018.
- [7] A. Brock, J. Donahue, and K. Simonyan, "Large scale gan training for high fidelity natural image synthesis," in *Proceedings of International Conference on Learning Representations*, 2018.
- [8] J. Donahue and K. Simonyan, "Large scale adversarial representation learning," in *Advances in Neural Information Processing Systems*, 2019.
- [9] T. Chen, X. Zhai, M. Ritter, M. Lucic, and N. Houlsby, "Self-supervised gans via auxiliary rotation loss," in *Proceedings of the IEEE Conference on Computer Vision and Pattern Recognition*, 2019.
- [10] J. Hoffman, E. Tzeng, T. Park, J. Zhu, P. Isola, K. Saenko, A. A. Efros, and T. Darrell, "Cycada: Cycle-consistent adversarial domain adaptation," in *Proceedings of the 35th International Conference on Machine Learning (ICML)*, 2018.
- [11] A. Makhzani and B. J. Frey, "Pixelgan autoencoders," in *Advances in Neural Information Processing Systems*, 2017.
- [12] D. P. Kingma and M. Welling, "Auto-encoding variational bayes," in *Proceedings of the 2nd International Conference on Learning Representations (ICLR)*, 2014.
- [13] I. Goodfellow, J. Pouget-Abadie, M. Mirza, B. Xu, D. Warde-Farley, S. Ozair, A. Courville, and Y. Bengio, "Generative adversarial nets," in *Advances in Neural Information Processing Systems (NeurIPS)*, 2014.
- [14] L. Clouâtre and M. Demers, "Figr: Few-shot image generation with reptile," *arXiv preprint arXiv:1901.02199*, 2019.
- [15] Y. Hong, L. Niu, J. Zhang, and L. Zhang, "Matchinggan: Matching-based few-shot image generation," in *Proceedings of IEEE International Conference on Multimedia and Expo (ICME)*, 2020.
- [16] Y. Hong, L. Niu, J. Zhang, W. Zhao, C. Fu, and L. Zhang, "F2gan: Fusing-and-filling gan for few-shot image generation," in *Proceedings of ACM Multimedia Conference on Multimedia Conference (ACM MM)*, 2020.
- [17] W. Liang, Z. Liu, and C. Liu, "Dawson: A domain adaptive few shot generation framework," *arXiv preprint arXiv:2001.00576*, 2020.
- [18] S. Bartunov and D. Vetrov, "Few-shot generative modelling with generative matching networks," in *Proceedings of International Conference on Artificial Intelligence and Statistics (AISTATS)*, 2018.
- [19] A. Antoniou, A. Storkey, and H. Edwards, "Data augmentation generative adversarial networks," *arXiv preprint arXiv:1711.04340*, 2017.
- [20] J. Zhu, R. Zhang, D. Pathak, T. Darrell, A. A. Efros, O. Wang, and E. Shechtman, "Toward multimodal image-to-image translation," in *Advances in Neural Information Processing Systems (NeurIPS)*, 2017.
- [21] E. Schwartz, L. Karlinsky, J. Shtok, S. Harary, M. Marder, A. Kumar, R. Feris, R. Giryes, and A. Bronstein, "Delta-encoder: an effective sample synthesis method for few-shot object recognition," in *Advances in Neural Information Processing Systems (NeurIPS)*, 2018.
- [22] I. Higgins, L. Matthey, A. Pal, C. Burgess, X. Glorot, M. Botvinick, S. Mohamed, and A. Lerchner, "beta-vae: Learning basic visual concepts with a constrained variational framework," in *Proceedings of 5th International Conference on Learning Representations (ICLR)*, 2017.
- [23] A. Almahairi, S. Rajeswar, A. Sordoni, P. Bachman, and A. C. Courville, "Augmented cyclegan: Learning many-to-many mappings from unpaired data," in *Proceedings of the 35th International Conference on Machine Learning (ICML)*, 2018.
- [24] Q. Mao, H.-Y. Lee, H.-Y. Tseng, S. Ma, and M.-H. Yang, "Mode seeking generative adversarial networks for diverse image synthesis," in *Proceedings of Conference on Computer Vision and Pattern Recognition (CVPR)*, 2019.
- [25] E. D. Cubuk, B. Zoph, D. Mane, V. K. Vasudevan, and Q. V. Le, "Autoaugment: Learning augmentation strategies from data," in *Proceedings of Conference on Computer Vision and Pattern Recognition (CVPR)*, 2019.
- [26] S. Lim, I. Kim, T. Kim, C. Kim, and S. Kim, "Fast autoaugment," in *Proceedings of Advances in Neural Information Processing Systems*, 2019.
- [27] D. Ho, E. Liang, X. Chen, I. Stoica, and P. Abbeel, "Population based augmentation: Efficient learning of augmentation policy schedules," in *Proceedings of International Conference on Machine Learning*, 2019.
- [28] K. Tian, C. Lin, M. Sun, L. Zhou, J. Yan, and W. Ouyang, "Improving auto-augment via augmentation-wise weight sharing," *Proceedings of Advances in Neural Information Processing Systems*, 2020.
- [29] L. Perez and J. Wang, "The effectiveness of data augmentation in image classification using deep learning," in *Proceedings of Conference on Computer Vision and Pattern Recognition (CVPR)*, 2017.
- [30] A. J. Ratner, H. Ehrenberg, Z. Hussain, J. Dunnmon, and C. Ré, "Learning to compose domain-specific transformations for data augmentation," in *Proceedings of Advances in neural information processing systems*, 2017.
- [31] H.-J. Jo, C.-H. Min, and J.-B. Song, "Bin picking system using object recognition based on automated synthetic dataset generation," in *2018 15th International Conference on Ubiquitous Robots (UR)*, 2018.
- [32] X. Zhang, Z. Wang, D. Liu, and Q. Ling, "DADA: Deep adversarial data augmentation for extremely low data regime classification," in *Proceedings of International Conference on Acoustics, Speech and Signal Processing (ICASSP)*, 2019.
- [33] N.-T. Tran, V.-H. Tran, N.-B. Nguyen, T.-K. Nguyen, and N.-M. Cheung, "On data augmentation for gan training," *IEEE Transactions on Image Processing (TIP)*, vol. 30, pp. 1882–1897, 2021.
- [34] Z. Chen, Y. Fu, Y. Zhang, Y.-G. Jiang, X. Xue, and L. Sigal, "Multi-level semantic feature augmentation for one-shot learning," *IEEE Transactions on Image Processing (TIP)*, vol. 28, no. 9, pp. 4594–4605, 2019.
- [35] B. Hariharan and R. B. Girshick, "Low-shot visual recognition by shrinking and hallucinating features," in *Proceedings of International Conference on Computer Vision (ICCV)*, 2017.
- [36] Z. Chen, Y. Fu, Y.-X. Wang, L. Ma, W. Liu, and M. Hebert, "Image deformation meta-networks for one-shot learning," in *Proceedings of the IEEE Conference on Computer Vision and Pattern Recognition*, 2019.
- [37] S. Tsutsui, Y. Fu, and D. Crandall, "Meta-reinforced synthetic data for one-shot fine-grained visual recognition," in *Proceedings of Advances in Neural Information Processing Systems*, 2019.
- [38] M. Dixit, R. Kwitt, M. Niethammer, and N. Vasconcelos, "AGA: attribute-guided augmentation," in *Proceedings of Conference on Computer Vision and Pattern Recognition (CVPR)*, 2017.
- [39] H. Gao, Z. Shou, A. Zareian, H. Zhang, and S. Chang, "Low-shot learning via covariance-preserving adversarial augmentation networks," in *Advances in Neural Information Processing Systems (NeurIPS)*, 2018.

- [40] Y. Wang, R. B. Girshick, M. Hebert, and B. Hariharan, "Low-shot learning from imaginary data," in *Proceedings of Conference on Computer Vision and Pattern Recognition (CVPR)*, 2018.
- [41] J. Liu, Y. Sun, C. Han, Z. Dou, and W. Li, "Deep representation learning on long-tailed data: A learnable embedding augmentation perspective," in *Proceedings of Conference on Computer Vision and Pattern Recognition (CVPR)*, 2020.
- [42] B. Lake, R. Salakhutdinov, J. Gross, and J. Tenenbaum, "One shot learning of simple visual concepts," in *Proceedings of the annual meeting of the cognitive science society (CogSci)*, 2011.
- [43] D. J. Rezende, S. Mohamed, I. Danihelka, K. Gregor, and D. Wierstra, "One-shot generalization in deep generative models," in *Proceedings of International Conference on Machine Learning (ICML)*, 2016.
- [44] S. Reed, Y. Chen, T. L. Paine, A. V. Den Oord, S. M. A. Eslami, D. J. Rezende, O. Vinyals, and N. De Freitas, "Few-shot autoregressive density estimation: towards learning to learn distributions," in *Proceedings of 6th International Conference on Learning Representations (ICLR)*, 2018.
- [45] A. Nichol, J. Achiam, and J. Schulman, "On first-order meta-learning algorithms," *arXiv preprint arXiv:1803.02999*, 2018.
- [46] C. Finn, P. Abbeel, and S. Levine, "Model-agnostic meta-learning for fast adaptation of deep networks," in *Proceedings of the 34th International Conference on Machine Learning (ICML)*, 2017.
- [47] O. Vinyals, C. Blundell, T. Lillicrap, D. Wierstra *et al.*, "Matching networks for one shot learning," in *Proceedings of Advances in neural information processing systems (NeurIPS)*, 2016.
- [48] Y. Pu, G. Zhe, R. Henao, Y. Xin, and L. Carin, "Variational autoencoder for deep learning of images, labels and captions," in *Advances in Neural Information Processing Systems (NeurIPS)*, 2016.
- [49] M. Mirza and S. Osindero, "Conditional generative adversarial nets," *arXiv preprint arXiv:1411.1784*, 2014.
- [50] M. Liu, X. Huang, A. Mallya, T. Karras, T. Aila, J. Lehtinen, and J. Kautz, "Few-shot unsupervised image-to-image translation," in *Proceedings of International Conference on Computer Vision (ICCV)*, 2019.
- [51] P. Isola, J.-Y. Zhu, T. Zhou, and A. A. Efros, "Image-to-image translation with conditional adversarial networks," in *Proceedings of Conference on Computer Vision and Pattern Recognition (CVPR)*, 2017.
- [52] J. Zhang, Y. Huang, Y. Li, W. Zhao, and L. Zhang, "Multi-attribute transfer via disentangled representation," in *Proceedings of The Thirty-Third AAAI Conference on Artificial Intelligence (AAAI)*, 2019.
- [53] C. Ledig, L. Theis, F. Huszar, J. Caballero, A. Cunningham, A. Acosta, A. P. Aitken, A. Tejani, J. Totz, Z. Wang, and W. Shi, "Photo-realistic single image super-resolution using a generative adversarial network," in *Proceedings of Conference on Computer Vision and Pattern Recognition (CVPR)*, 2017.
- [54] J. Johnson, A. Alahi, and L. Fei-Fei, "Perceptual losses for real-time style transfer and super-resolution," in *Proceedings of the European Conference on Computer Vision (ECCV)*, 2016.
- [55] J. Xin, N. Wang, X. Gao, and J. Li, "Residual attribute attention network for face image super-resolution," in *Proceedings of The Thirty-Third AAAI Conference on Artificial Intelligence (AAAI)*, 2019.
- [56] Y. Zhang, P. David, H. Foroosh, and B. Gong, "A curriculum domain adaptation approach to the semantic segmentation of urban scenes," *PAMI*, vol. 42, no. 8, pp. 1823–1841, 2020.
- [57] T. R. Shaham, T. Dekel, and T. Michaeli, "Singan: Learning a generative model from a single natural image," in *Proceedings of International Conference on Computer Vision (ICCV)*, 2019.
- [58] X. Zhang, J. Mao, Y. Li, W. T. Freeman, J. B. Tenenbaum, and J. Wu, "Program-guided image manipulators," in *Proceedings of International Conference on Computer Vision (ICCV)*, 2019.
- [59] A. Shocher, S. Bagon, P. Isola, and M. Irani, "Ingan: Capturing and retargeting the "dna" of a natural image," in *Proceedings of International Conference on Computer Vision (ICCV)*, 2019.
- [60] X. Huang and S. J. Belongie, "Arbitrary style transfer in real-time with adaptive instance normalization," in *Proceedings of International Conference on Computer Vision (ICCV)*, 2017.
- [61] L. A. Gatys, A. S. Ecker, and M. Bethge, "Image style transfer using convolutional neural networks," in *Proceedings of Conference on Computer Vision and Pattern Recognition (CVPR)*, 2016.
- [62] L. Ma, X. Jia, Q. Sun, B. Schiele, T. Tuytelaars, and L. V. Gool, "Pose guided person image generation," in *Advances in Neural Information Processing Systems (NeurIPS)*, 2017.
- [63] Z. Zhu, T. Huang, B. Shi, M. Yu, B. Wang, and X. Bai, "Progressive pose attention transfer for person image generation," in *Proceedings of Conference on Computer Vision and Pattern Recognition (CVPR)*, 2019.
- [64] J. Bao, D. Chen, F. Wen, H. Li, and G. Hua, "CVAE-GAN: fine-grained image generation through asymmetric training," in *Proceedings of International Conference on Computer Vision (ICCV)*, 2017.
- [65] T. Miyato and M. Koyama, "cgans with projection discriminator," in *Proceedings of 6th International Conference on Learning Representations (ICLR)*, 2018.
- [66] A. Odena, C. Olah, and J. Shlens, "Conditional image synthesis with auxiliary classifier GANs," in *Proceedings of the 34th International Conference on Machine Learning (ICML)*, 2017.
- [67] G. Cohen, S. Afshar, J. Tapson, and A. van Schaik, "EMNIST: an extension of MNIST to handwritten letters," in *Proceedings of International Joint Conference on Neural Networks (IJCNN)*, 2017.
- [68] Q. Cao, L. Shen, W. Xie, O. M. Parkhi, and A. Zisserman, "Vggface2: A dataset for recognising faces across pose and age," in *Proceedings of 13th IEEE International Conference on Automatic Face & Gesture Recognition (FG)*, 2018.
- [69] M.-E. Nilsback and A. Zisserman, "Automated flower classification over a large number of classes," in *Proceedings of Sixth Indian Conference on Computer Vision, Graphics & Image Processing (CVGIP)*, 2008.
- [70] J. Deng, W. Dong, R. Socher, L.-J. Li, K. Li, and L. Fei-Fei, "Imagenet: A large-scale hierarchical image database," in *Proceedings of Conference on Computer Vision and Pattern Recognition (CVPR)*, 2009.
- [71] G. Van Horn, S. Branson, R. Farrell, S. Haber, J. Barry, P. Ipeirotis, P. Perona, and S. Belongie, "Building a bird recognition app and large scale dataset with citizen scientists: The fine print in fine-grained dataset collection," in *Proceedings of Conference on Computer Vision and Pattern Recognition (CVPR)*, 2015.
- [72] Y. Kawano and K. Yanai, "Automatic expansion of a food image dataset leveraging existing categories with domain adaptation," in *Proceedings of the European Conference on Computer Vision (ECCV)*, 2014.
- [73] L. M. Mescheder, A. Geiger, and S. Nowozin, "Which training methods for gans do actually converge?" in *Proceedings of the 35th International Conference on Machine Learning (ICML)*, 2018.
- [74] F. Sung, Y. Yang, L. Zhang, T. Xiang, P. H. Torr, and T. M. Hospedales, "Learning to compare: Relation network for few-shot learning," in *Proceedings of Conference on Computer Vision and Pattern Recognition (CVPR)*, 2018.
- [75] Q. Sun, Y. Liu, T.-S. Chua, and B. Schiele, "Meta-transfer learning for few-shot learning," in *Proceedings of Conference on Computer Vision and Pattern Recognition (CVPR)*, 2019.
- [76] W. Li, L. Wang, J. Xu, J. Huo, Y. Gao, and J. Luo, "Revisiting local descriptor based image-to-class measure for few-shot learning," in *Proceedings of Conference on Computer Vision and Pattern Recognition (CVPR)*, 2019.
- [77] H. Tseng, H. Lee, J. Huang, and M. Yang, "Cross-domain few-shot classification via learned feature-wise transformation," in *Proceedings of 8th International Conference on Learning Representations (ICLR)*, 2020.
- [78] L. Yang, L. Li, Z. Zhang, X. Zhou, E. Zhou, and Y. Liu, "Dpgn: Distribution propagation graph network for few-shot learning," in *Proceedings of Conference on Computer Vision and Pattern Recognition (CVPR)*, 2020.
- [79] C. Zhang, Y. Cai, G. Lin, and C. Shen, "Deepemd: Few-shot image classification with differentiable earth mover's distance and structured classifiers," in *Proceedings of Conference on Computer Vision and Pattern Recognition (CVPR)*, 2020.
- [80] X. Li, J. Wu, Z. Sun, Z. Ma, J. Cao, and J.-H. Xue, "Bsnet: Bi-similarity network for few-shot fine-grained image classification," *IEEE Transactions on Image Processing (TIP)*, 2020.
- [81] M. Heusel, H. Ramsauer, T. Unterthiner, B. Nessler, and S. Hochreiter, "GANs trained by a two time-scale update rule converge to a local nash equilibrium," in *Advances in Neural Information Processing Systems (NeurIPS)*, 2017.
- [82] R. Zhang, P. Isola, A. A. Efros, E. Shechtman, and O. Wang, "The unreasonable effectiveness of deep features as a perceptual metric," in *Proceedings of Conference on Computer Vision and Pattern Recognition (CVPR)*, 2018.
- [83] K. He, X. Zhang, S. Ren, and J. Sun, "Deep residual learning for image recognition," in *Proceedings of Conference on Computer Vision and Pattern Recognition (CVPR)*, 2016.